



Preparation of FeS@Fe₃O₄ core–shell magnetic nanoparticles and their application in uranyl ions removal from aqueous solution

Yan Liu² · Pengfei Yang^{1,2} · Qi Li¹ · Ying Liu¹ · Jiang Yin¹

Received: 16 March 2019 / Published online: 24 June 2019
© Akadémiai Kiadó, Budapest, Hungary 2019

Abstract

FeS@Fe₃O₄ magnetic nanoparticles were prepared by ultrasonic-assisted method and characterized by TEM, FTIR, XRD, SEM, EDS, BET and VSM. The factors affecting the adsorption properties of uranyl ions by FeS@Fe₃O₄ were studied. Results show that the FeS@Fe₃O₄ nanoparticles have core–shell structure and superparamagnetism. Under the optimized conditions, the maximum adsorption capacity can reach 229.03 mg/g. The optimum adsorption conditions were as follows: pH=6, temperature 80 °C, C₀=35 mg/L, contact time 2.5 h, adsorbent dosage 10 mg. Adsorption kinetics and thermodynamic studies show that the adsorption process accords with the Freundlich isotherm adsorption model and the pseudo-second-order kinetic model.

Keywords FeS · Fe₃O₄ · Nanoparticles · Adsorption · Uranyl ions

Introduction

The rapid growth of energy is partly due to the development of nuclear technology. Uranium is an important nuclear fuel which is inevitably released into the environment in the process of exploitation and utilization [1]. Uranyl ions in aqueous solution have high radioactivity, high mobility and biotoxicity, which bring immeasurable harm to human beings and the environment [2]. Therefore, it is of great significance to find an economical and friendly method for the treatment of uranium-containing wastewater. Currently, these methods to treat uranium-containing wastewater include chemical precipitation [3–5], electrochemical treatment [6], solvent extraction [7–10], membrane separation [11, 12] and adsorption [13, 14] and so on. Among the above methods, the adsorption method is one of the most economical, reusable and easy-to-use methods, and has attracted more and more attention [15].

In recent years, studies have shown that nano-metal sulfides, as adsorbents, have the advantages of fast adsorption speed, strong adsorption capacity, and good adsorption properties to heavy metal ions, radioactive elements and organic compounds in water and soil substrates, and have potential research and application value [16–20]. Fang et al. [21] used zinc sulfide nanocrystals to remove and separate heavy metal ions in wastewater. The results showed that the adsorption capacities of zinc sulfide nanocrystals to Hg²⁺, Cu²⁺, Pb²⁺ and Cd²⁺ in wastewater were 475 mg/g, 384 mg/g, 52 mg/g and 82 mg/g, respectively. Sun et al. [22] used iron sulphide (FeS) nanoparticles to treat Hg(II)-containing wastewater, and the maximum adsorption capacity reached 1989 mg/g. However, nano-metal sulfides also have some disadvantages, for example, it is easy to aggregate in aqueous solution, and it is difficult to separate from wastewater after adsorption of heavy metal ions. These shortcomings restrict its engineering application to a certain extent. Therefore, it is necessary to modify the existing materials [23–28].

In this paper, FeS@Fe₃O₄ magnetic nanoparticles with core–shell structure and superparamagnetism were prepared by ultrasonic assisted method. The physicochemical properties of FeS@Fe₃O₄ magnetic nanoparticles were detected by TEM, FTIR, XRD, EDS, SEM, BET and VSM. And the adsorption properties of FeS@Fe₃O₄ magnetic nanoparticles for uranyl ions were investigated. The adsorption types

✉ Pengfei Yang
ypengfei2008@126.com

¹ School of Chemistry and Chemical Engineering, University of South China, Hengyang 421001, China

² Hunan Engineering Laboratory for Preparation Technology of Polyvinyl Alcohol Fiber Material, Huaihua University, Huaihua 418000, China

were analyzed from the aspects of kinetic, isotherms, and thermodynamic.

Experimental

Materials

UO₂ (NO₃)₂·6H₂O was from Chushengwei Chemical Technology Co., Ltd. Anhydrous ferric chloride (FeCl₃, > 99%) was from Sinopharm Chemical Reagent Co., Ltd (China). Iron(II) chloride tetrahydrate (FeCl₂·4H₂O, > 99%) came from Tianjin Fengchuan Chemical Reagent Technologies Co., Ltd. Sodium sulfide nonahydrate (Na₂S·9H₂O, > 98%), Ethyl alcohol absolute (CH₂CH₃OH, > 99%) and Ammonia solution (NH₃·H₂O, 25–28%) was purchased from Tianjin Hongyan Chemical Reagent Factory (China), Hunan Huihong and Guandong Guanghua, respectively. The other chemicals were purchased from other Chinese reagent companies. Deionized water was homemade. All chemical purchased were analytical grade and used as received without any pretreatment.

Analytical methods

Bruker D8 powder X-ray diffractometer (XRD) was used to identify the phases of samples. Nicolet-460 Fourier Infrared Spectrometer (FT-IR) was used to detect the structure of samples and chemical bonds in it. The morphologies of samples were observed by Tecnai G20 transmission electron microscopy (TEM) and JSM-7500F scanning electron microscopy (SEM). The components and elements of samples were determined by Oxford X-Max EDS meter (EDS). The magnetic intensity of adsorbent was detected by Squid-Vibrating sample magnetometer (VSM). T6 Xinrui visible spectrophotometer was carried out measure uranium concentration in solution.

Preparation of magnetic Fe₃O₄ nanoparticles

1.3 g FeCl₃ was dissolved in 140 mL deionized water in a 250 mL beaker. The above mixture was treated by ultrasonic treatment for 15 min and deoxidized with N₂ for 30 min.

Then 1.1 g FeCl₂·4H₂O was added in the above solution and the mixture were stirred quickly until completely dissolved. 0.4 g sodium dodecyl benzene sulfonate (SDBS) was dissolved in 5 mL deionized water then the SDBS solution was added into the above mixture solution to prevent Fe₃O₄ nanoparticles from agglomerating. Afterwards, 30 mL 2 M ammonia solution was dropped into the obtained solution in the three-necked flask until the pH value was between 9 and 10. Meanwhile, under the protection of N₂, the mixture solution was being stirred

vigorously at a speed of 1000 rpm and kept for 30 min. After stirring, the final black solution aged for 30 min in the 60 °C water. Then the resulting product was separated from solution in an external magnetic field and washed for three times with deionized water and ethanol, respectively, until the pH of filtered solution reached 7. Finally, the black precipitate was dried in a vacuum drying chamber at 60 °C for 6 h.

Preparation of Fe₃O₄@FeS

0.2 g Fe₃O₄ was dispersed in 10 mL deionized water and transferred to 50 mL beaker. In order to improve the dispersibility of the synthesized nanocomposites, 0.9 mL 7.4% carboxyl methyl cellulose (CMC) solution was also added into the above solution and the mixture solution was ultrasonic treated for 30 min. After ultrasonic treatment, 1.4 g Na₂S·9H₂O was dissolved in above solution and further ultrasonic treatment was carried out for 10 min. Then 0.6 g FeCl₂·4H₂O was dissolved in the 10 mL deoxidized deionized water, and added dropwise to the above solution under N₂ protection. At the same time, the mixture solution was stirred, and then the obtained mixture solution was ultrasonic treated for 30 min. Finally, the product was washed several times with deionized water. The product was then dried in a vacuum drying chamber at 60 °C for 6 h.

Adsorption experiments

The effects of pH, temperature, contact time, adsorbent dose and initial concentration of uranyl ions on the absorption efficiency were investigate by batch experiments. 10 mg adsorbents were added into a series of 80 mL 35 mg/L uranyl ions solutions in the conical flasks then the above conical flasks all were put in a thermostatic oscillator set at 80 °C then shaken for 2.5 h at constant temperature until the achievement of adsorption equilibrium. The solid phase was separated from the solution by an external magnet, and the concentration of uranyl ion in the supernatant was detected by visible light spectrophotometer, respectively. The adsorption capacity (q_e) and the removal rate (A) were calculated according to the following formula [29].

$$q_e = (C_0 - C_e)V/M \quad (1)$$

$$A(\%) = (C_0 - C_e)/C_0 \times 100 \quad (2)$$

where C_0 (mg/L) is the initial concentration of uranyl ions. C_e (mg/L) is the remnant concentration of uranyl ions in the supernatant after absorption. V (L) is the volume of aqueous solution. M (g) is the adsorbent dose.

Desorption experiments

In order to explore reusability of the absorbent, desorption experiments were carried out. 10 mg absorbent was desorbed with 10 mL 1.5 mol/L Na_2CO_3 solution at a temperature of 80 °C, and the mixture was placed in a thermostatic oscillator and shaken for 2.5 h. After desorption, the absorbent was separated from the solution by magnetic separation and the concentration of uranyl ions in supernatant was measured by visible light spectrophotometer. Finally, the adsorbent was washed with distilled water until it reached a neutral state and left for the next round of adsorption–desorption experiments.

Interference experiment

The effect of competitive ions including Ni^{2+} , Mg^{2+} , Zn^{2+} , Al^{3+} and Cu^{2+} on the absorption efficiency of uranyl ions were investigated. A series of different concentrations of Ni^{2+} , Mg^{2+} , Zn^{2+} , Al^{3+} , Cu^{2+} were mixed with 10 mL 35 mg/L uranyl ions solution, respectively, and desorbed at 80 °C for 2.5 h.

Results and discussion

Characterization

The XRD patterns ($10^\circ < 2\theta < 90^\circ$) of Fe_3O_4 , $\text{FeS}@Fe_3O_4$ and U-laden $\text{FeS}@Fe_3O_4$ were shown in Fig. 1. The six characteristic peaks of Fe_3O_4 at 2θ values of 30.32°, 35.40°, 43.26°, 53.80°, 57.36° and 62.96° correspond to crystal planes (220), (311), (400), (422), (511) and (440) according

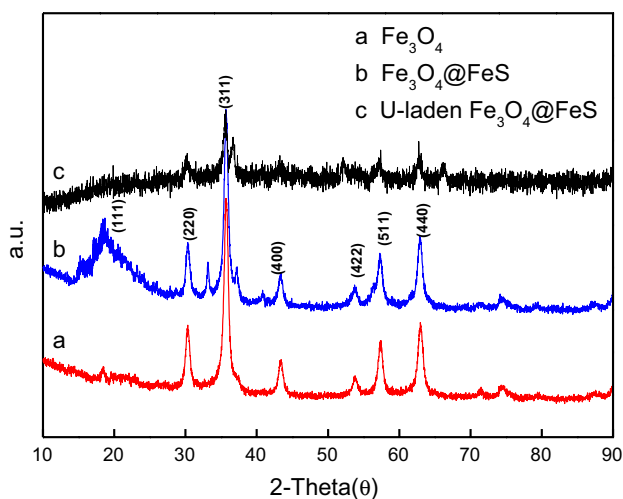


Fig. 1 XRD analysis of Fe_3O_4 , $\text{FeS}@Fe_3O_4$ and U-laden $\text{FeS}@Fe_3O_4$

to JCPDS card No.19-0629. In the XRD pattern of the $\text{FeS}@Fe_3O_4$, the above six characteristic peaks did not change significantly, which means that the coating of FeS did not change the structure of Fe_3O_4 . However, the XRD pattern of $\text{FeS}@Fe_3O_4$ exhibits two new XRD characteristic peaks at 2θ values of 18.4° and 33.3°, which correspond to the XRD characteristic peaks of FeS [30]. A broad peak of about 18.4° can be observed, which indicates that the crystal of FeS is not well crystallized and the crystal may be nano-sized [31, 32]. In the XRD pattern of U-laden $\text{FeS}@Fe_3O_4$, according to JCPDS card No.24-0749, the new characteristic XRD peak at 2θ values of 36.2°, 52.2° and 65.8° is attributed to the adsorption of uranyl ions. And in this diffraction, all peaks of Fe_3O_4 and FeS are weakened, which means that a large amount of uranyl ions are successfully adsorbed on the adsorbents.

The FT-IR spectra of Fe_3O_4 , $\text{FeS}@Fe_3O_4$ and U-laden $\text{FeS}@Fe_3O_4$ are shown in Fig. 2. As shown in the figure, there are two peaks at 3400 cm^{-1} and 570 cm^{-1} in the spectrum of the three samples, which belong to the O–H stretching bond and the Fe–O bond, respectively [33]. In addition, a broad peak in the Fe_3O_4 spectrum at 1072 cm^{-1} splits into two peaks at 1094 cm^{-1} and 1019 cm^{-1} in the $\text{FeS}@Fe_3O_4$ spectrum, which may be due to the local deformation of the lattice caused by the coating of FeS [34]. In U-laden $\text{FeS}@Fe_3O_4$ spectrum, these two peaks are moved to 1094 cm^{-1} and 1019 cm^{-1} , which is mainly due to the adsorption of uranyl ions by $\text{FeS}@Fe_3O_4$ [35, 36].

The magnetic properties of $\text{FeS}@Fe_3O_4$ nanoparticles were measured at room temperature by using an external magnetic field of $-20 \text{ k Oe} \leq H \leq 20 \text{ k Oe}$. The results are shown in Fig. 3. The saturation magnetization of $\text{FeS}@Fe_3O_4$ can be clearly observed in the curve, about

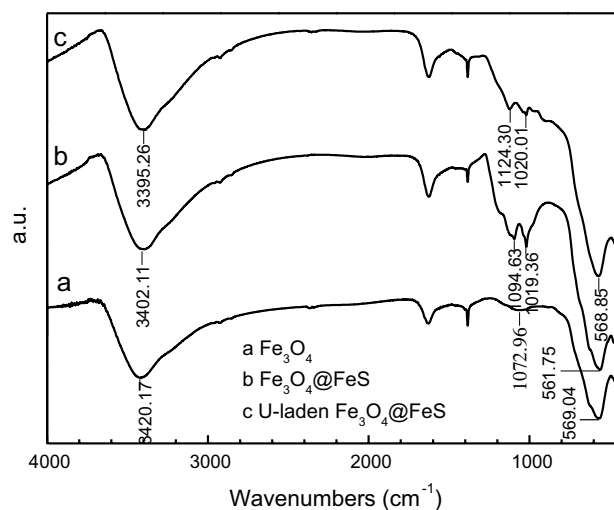


Fig. 2 FT-IR spectrum of Fe_3O_4 , $\text{FeS}@Fe_3O_4$ and U-laden $\text{FeS}@Fe_3O_4$

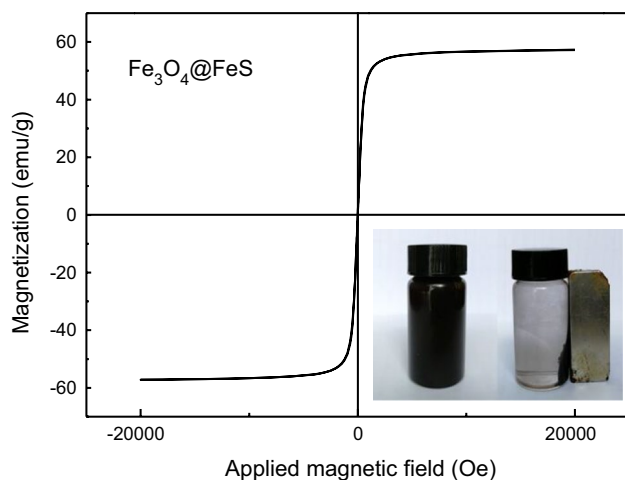


Fig. 3 Magnetic hysteresis loop of $\text{FeS@Fe}_3\text{O}_4$ and the photographs of magnetic separation of $\text{FeS@Fe}_3\text{O}_4$ (inset)

57.18 emu/g, which is lower than the saturation magnetization of Fe_3O_4 reported in many literatures which is 90 emu/g [37]. This may be attributed to the encapsulation of FeS and quantum size effects. There is no coercivity and no residual magnetism nearly in the magnetic hysteresis loop and the superparamagnetism of $\text{FeS@Fe}_3\text{O}_4$ could be

proved [38]. The incidental pattern in the lower right corner indicates that $\text{FeS@Fe}_3\text{O}_4$ has an excellent magnetic response to the external magnet and can be separated by an external magnet within 10 s.

EDS analysis was used to determine the main elements in the $\text{FeS@Fe}_3\text{O}_4$ and U-laden $\text{FeS@Fe}_3\text{O}_4$. As clearly exhibited in Fig. 4, the distributions of main elements of the $\text{FeS@Fe}_3\text{O}_4$ and U-laden $\text{FeS@Fe}_3\text{O}_4$ can be observed obviously. The presence of sulfur elements in $\text{FeS@Fe}_3\text{O}_4$ (Fig. 4a) attests to the successful loading of FeS on the Fe_3O_4 surface. In the Fig. 4b, the presence of uranium element could be obviously observed and the wt % of U reached 3.68%. It is proved that $\text{FeS@Fe}_3\text{O}_4$ has good adsorption ability for uranyl ion.

The morphology of Fe_3O_4 and $\text{FeS@Fe}_3\text{O}_4$ were characterized by transmission electron microscope (TEM). The morphology of U-laden $\text{FeS@Fe}_3\text{O}_4$ was characterized by scanning electron microscope (SEM). As shown in Fig. 5, the morphology of Fe_3O_4 is sphere-like and its size is about 10–20 nm. In Fig. 5b, the Fe_3O_4 nanoparticles are coated with FeS, and the core-shell structure of $\text{FeS@Fe}_3\text{O}_4$ can be proved. As shown in Fig. 5c, the white materials on the surface of U-laden $\text{FeS@Fe}_3\text{O}_4$ is the crystal of uranyl ion adsorbed on it, which proves that uranyl ion is successfully adsorbed by the $\text{FeS@Fe}_3\text{O}_4$ nanoparticles.

Fig. 4 EDS analysis of $\text{FeS@Fe}_3\text{O}_4$ (a) and U-adsorbed $\text{FeS@Fe}_3\text{O}_4$ (b)

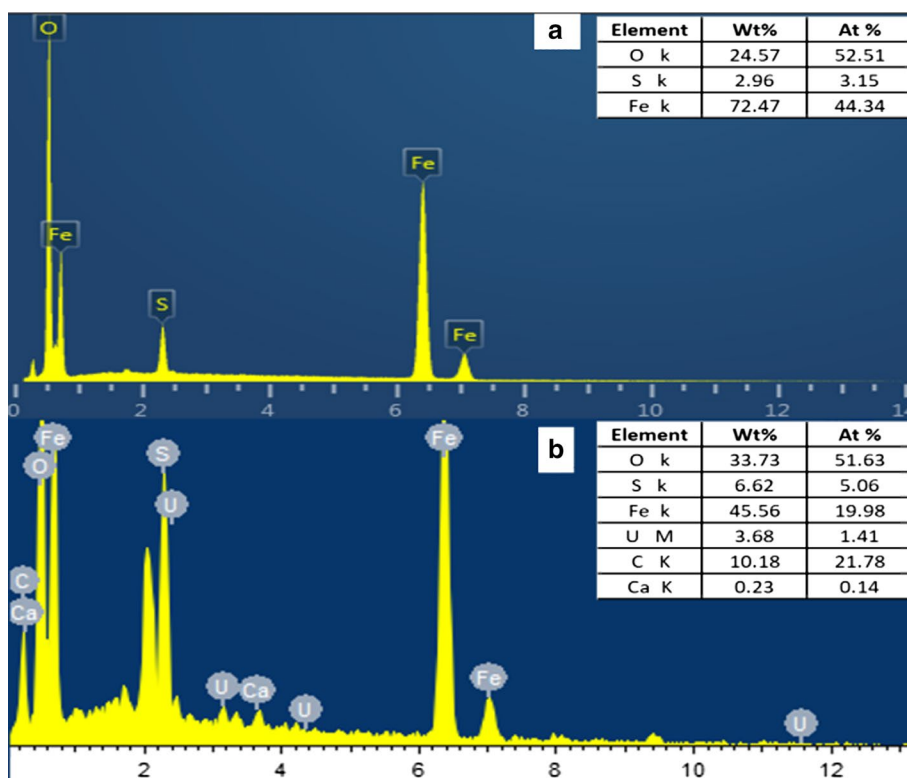
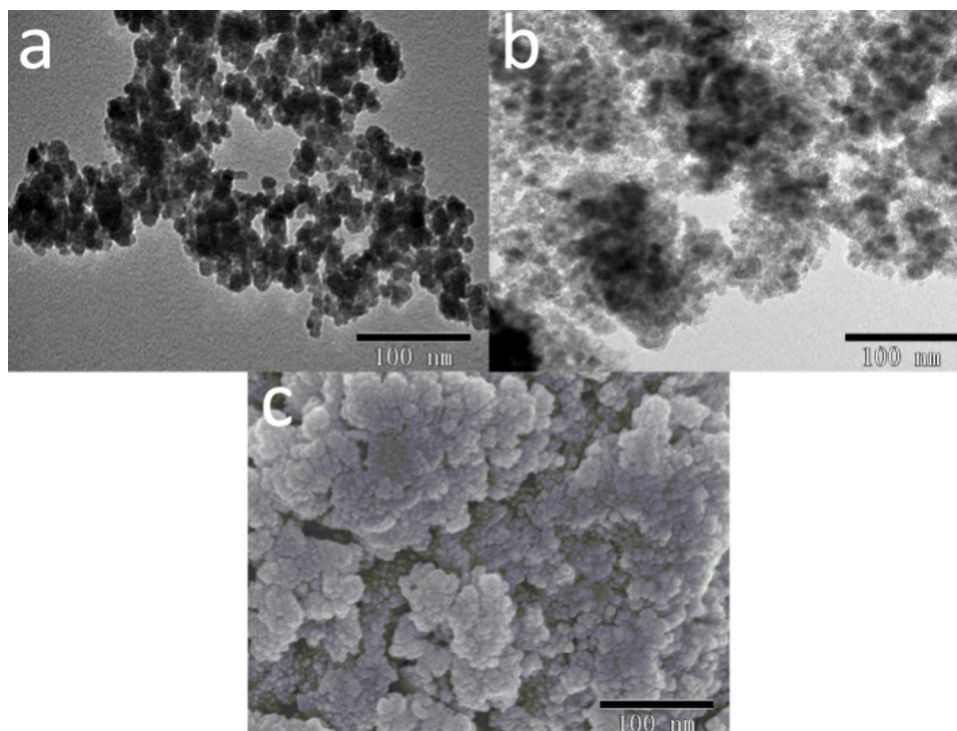


Fig. 5 TEM images of Fe_3O_4 (a), $\text{FeS}@Fe_3\text{O}_4$ (b), and SEM image of U-laden $\text{FeS}@Fe_3\text{O}_4$ (c)



A comparison of adsorption capacity for uranyl ions between Fe_3O_4 , FeS and $\text{Fe}_3\text{O}_4@FeS$

80 mL 35 mg/g uranyl ion solution was added to each of the three conical flasks, the pH of the solution was adjusted to 6, and then 10 mg Fe_3O_4 , FeS and $\text{FeS}@Fe_3\text{O}_4$ were added, respectively, and these solutions were shaken for 2.5 h at 80 °C in a thermostatic oscillator. The supernatants of the three solutions were taken out at different adsorption time, and the uranyl ion concentration was measured to calculate the adsorption capacity and the adsorption rate. The adsorption properties of Fe_3O_4 , FeS and $\text{FeS}@Fe_3\text{O}_4$ for uranyl ions are shown in Fig. 6. It can be seen from the figure that the adsorption capacities of Fe_3O_4 and FeS are 154.0 mg/g and 211.0 mg/g, respectively. The adsorption capacity of $\text{FeS}@Fe_3\text{O}_4$ nanocomposites is 229.03 mg/g, which is 48.7% higher than that of Fe_3O_4 nanoparticles and 8.6% higher than that of FeS nanoparticles. This is because FeS is easy to aggregate when it is present alone, which greatly reduces its adsorption capacity. When the FeS is encapsulated on the Fe_3O_4 nanoparticles, the composite adsorbent becomes dispersed and more stable, and therefore, the adsorbent can provide a larger surface area and facilitate adsorption. According to the specific surface area test results, the specific surface area of FeS was 29.0264 m^2/g , and the specific surface area of $\text{FeS}@Fe_3\text{O}_4$ was 82.4732 m^2/g . It is proved that $\text{FeS}@Fe_3\text{O}_4$ has better adsorption performance for uranyl ions than Fe_3O_4 and FeS.

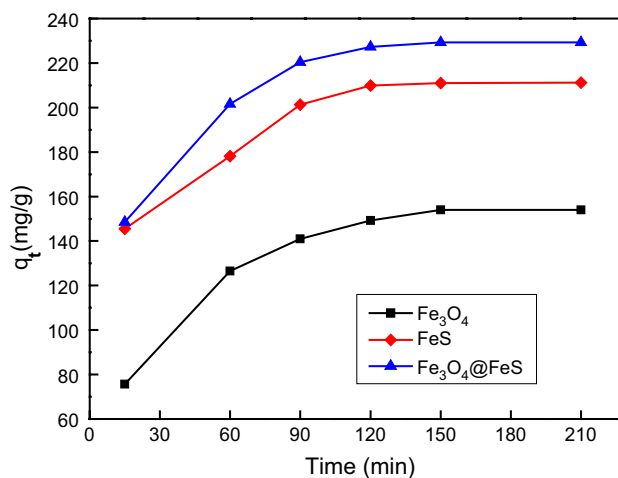


Fig. 6 Comparison of adsorption capacity for uranyl ions between Fe_3O_4 , FeS and $\text{Fe}_3\text{O}_4@FeS$ (pH=6, $m=10$ mg, $T=80$ °C, $C_0=35$ mg/L, $V=80$ mL)

Effect of the contact time

In order to study the effect of contact time on the adsorption of uranyl ions by $\text{FeS}@Fe_3\text{O}_4$, the contact time was from 15 to 210 min, the adsorption dosage was 10 mg, the initial uranyl ion concentration was 35 mg/L, the volume of the solution was 80 mL, the pH of solution was 6 and the temperature was 80 °C, under these conditions, a series of adsorption experiments were carried out. The results are shown in

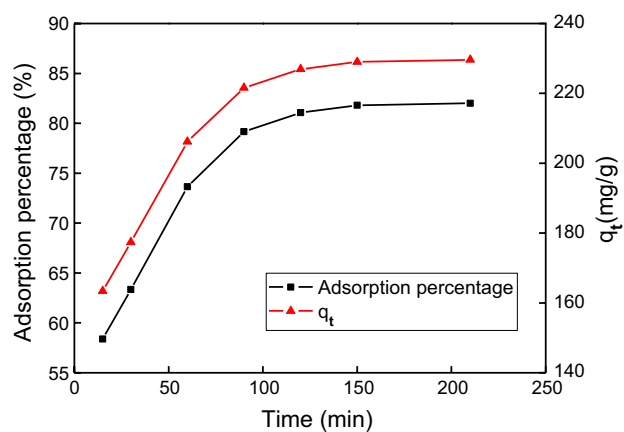


Fig. 7 Effect of adsorption time on the adsorption of uranyl ions by FeS@Fe₃O₄ (pH=6, $m=10$ mg, $T=80$ °C, $C_0=35$ mg/L, $V=80$ mL)

Fig. 7. As can be seen from the figure, with the increase of the contact time, the adsorption rate and the adsorption capacity increase rapidly. When the adsorption process reaches 150 min, the adsorption process reaches the adsorption equilibrium, and the adsorption rate reaches 81.8%, and remains basically unchanged in the subsequent time. This is because the adsorption of uranyl ions by FeS@Fe₃O₄ is firstly caused by diffusion of uranyl ions into the outer surface of the material, followed by transfer from the outer surface to the inner surface [39]. The adsorption process takes a longer time. Therefore, the adsorption rate and the adsorption capacity of uranyl ions by FeS@Fe₃O₄ increases with time until the adsorption equilibrium is reached. And the maximum adsorption capacity is 229.03 mg/g.

Effect of the adsorbent dosage

To investigate the effect of adsorbent dosage on the adsorption of uranyl ions by FeS@Fe₃O₄, the dosage of FeS@Fe₃O₄ was from 5 to 25 mg, the contact time was 150 min, the initial uranyl ion concentration was 35 mg/L, the volume of the solution was 80 mL, the pH of solution was 6 and the temperature was 80 °C, under these conditions, a series of adsorption experiments were carried out. The results are shown in Fig. 8. As can be seen from the figure that with the increase of initial uranyl ion concentration, the adsorption capacity of FeS@Fe₃O₄ to uranyl ion increases and the adsorption rate decreases. When the dosage of adsorbent is 10 mg, the adsorption rate reaches 81.8% and the adsorption capacity is 229.03 mg/L. When the dosage of adsorbent is 20 mg, the adsorption rate reaches 82.4% and the adsorption capacity is 115.29 mg/L. The main reason is that the content of uranyl ion in uranyl solution is constant. With the increase of adsorbent dosage, the number of effective adsorption active sites increases, and the removal rate of uranyl ion increases, but the amount of uranyl ion adsorbed by unit

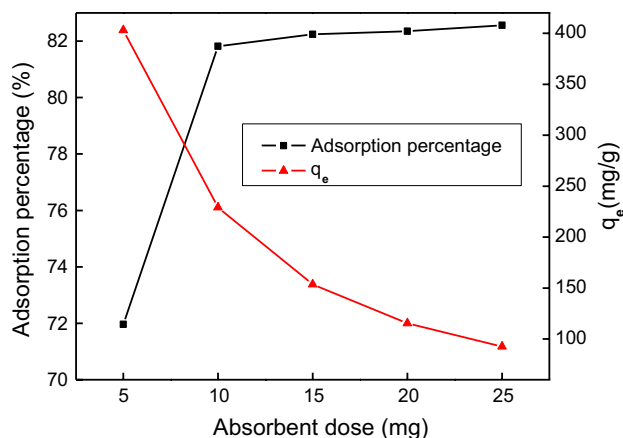


Fig. 8 Effect of adsorbent dose on the adsorption of uranyl ions by FeS@Fe₃O₄ (pH=6, $t=150$ min, $T=80$ °C, $C_0=35$ mg/L, $V=80$ mL)

mass FeS@Fe₃O₄ decreases [40]. The adsorption capacity of adsorbents per unit mass was decreased. When the dosage of the adsorbent is more than 10 mg, the removal rate with the addition of the adsorbent is increased, but the adsorption capacity of the unit mass of the adsorbent is decreased rapidly. From the optimal point of view, the optimal dosage of the adsorbent is 10 mg.

Effect of pH

The pH value of uranyl ion solution was adjusted with nitric acid and sodium hydroxide solutions. In order to study the effect of pH on the adsorption of uranyl ions by FeS@Fe₃O₄, the pH of solution was from 2 to 8, the contact time was 150 min, the adsorption dosage was 10 mg, the initial uranyl ion concentration was 35 mg/L, the volume of the solution was 80 mL and the temperature was 80 °C, under these conditions, a series of adsorption experiments were carried out. The results are shown in Fig. 9. It is obvious that when the pH value changes from 2 to 5, the adsorption efficiency of FeS@Fe₃O₄ for uranyl ions increases with the increase of pH value. When the pH value is 6, the adsorption efficiency reaches the maximum value. After that, with the increase of pH ($pH > 6$), the adsorption efficiency begins to decrease slightly. The main reason for the above phenomenon is that the degree of protonation is different in different pH solutions [41, 42]. In the solution with lower pH, the degree of protonation is greater, and H⁺ in the solution is competitive with UO₂²⁺ for adsorption, which affects the adsorption performance of uranyl ion by FeS@Fe₃O₄, which results in the low adsorption capacity and removal rate of uranyl ion by FeS@Fe₃O₄. On the other hand, there are different forms of uranium in different pH. In the case of pH=6, the uranium in solution mainly exists in the form

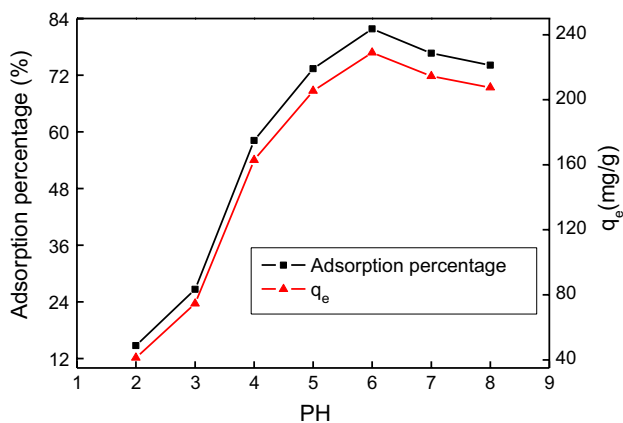


Fig. 9 Effect of pH on the adsorption of uranyl ions by FeS@Fe₃O₄ ($m = 10$ mg, $t = 150$ min, $T = 80$ °C, $C_0 = 35$ mg/L, $V = 80$ mL)

of UO₂²⁺. In this case, the adsorption ability of FeS@Fe₃O₄ is the strongest. With the increase of pH, OH⁻ and UO₂²⁺ form ions with lower adsorption affinity, including [UO₂OH]⁺, [(UO₂)₃(OH)₄]²⁺, [(UO₂)₂OH]³⁺, [(UO₂)₃OH]³⁺, [(UO₂)₄OH]⁷⁺, [UO₂(OH)₄]²⁻, [(UO₂)₃(OH)₇]⁻ [43], which reduce the adsorption amount of uranyl ion, resulting in the decrease of adsorption capacity and removal rate of uranyl ion by FeS@Fe₃O₄. Therefore, the solution pH = 6 is chosen as the optimal reaction condition.

Effect of temperature

Temperature was also an important parameter. A series of experiments were performed in 80 35 mg/L of the uranyl ions solutions (adjusted pH = 6) under different temperature ranging from 30 to 90 °C. 10 mg adsorbent was added into the above solution and shaken for 2.5 h at 80 °C. Figure 10

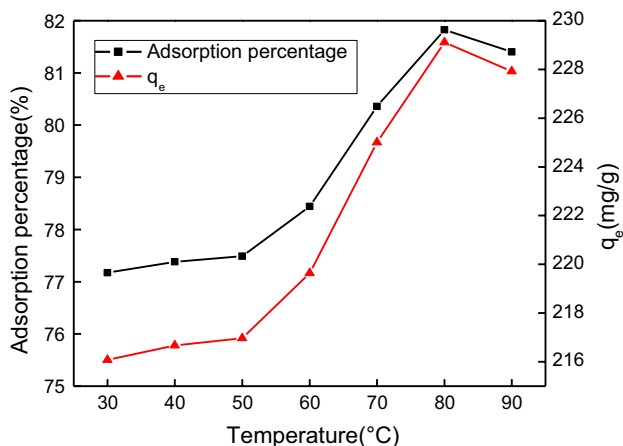


Fig. 10 Effect of temperature on the adsorption of uranyl ions by FeS@Fe₃O₄ ($m = 10$ mg, $t = 150$ min, pH = 6, $C_0 = 35$ mg/L, $V = 80$ mL)

shows that when the temperature is less than 80 °C, the adsorption capacity and removal rate of uranyl ion by FeS@Fe₃O₄ increase with temperature increasing, and when the temperature is higher than 80 °C, The adsorption capacity and removal rate of uranyl ion by FeS@Fe₃O₄ decreased slightly with temperature increasing. As the temperature increases, it is advantageous for the adsorbed molecules to diffuse from the outer surface to the inner surface of the adsorbent, so that the surface of the adsorbent can provide more active sites, thereby increasing the amount of adsorption. The adsorption of uranyl ions by FeS@Fe₃O₄ contains chemical adsorption and physical adsorption. As the temperature gradually increases, the physical adsorption efficiency decreases and the chemisorption reaches equilibrium. Therefore, when the temperature exceeds 80 °C, the adsorption capacity of FeS@Fe₃O₄ for uranyl ions is slightly decreased. Therefore, the optimum adsorption temperature is 80 °C.

Effect of the initial concentration of uranyl ions

In order to study the effect of initial uranyl ion concentration on the adsorption of uranyl ions by FeS@Fe₃O₄, the initial uranyl ion concentration was from 10 to 60 mg/L, the pH of solution was 6, the contact time was 150 min, the adsorption dosage was 10 mg, the volume of the solution was 80 mL and the temperature was 80 °C, under these conditions, a series of adsorption experiments were carried out. The results are shown in Fig. 11. It can be seen from Fig. 11 that as the initial uranyl ion concentration increases, the adsorption capacity of FeS@Fe₃O₄ on uranyl ions increases, and the adsorption rate decreases. This is because when the initial concentration of uranyl ions is low, the adsorption of uranyl ions by the adsorbent is far from saturation, so the removal rate is high and the adsorption amount is low. As the initial uranyl ion concentration increases, and the

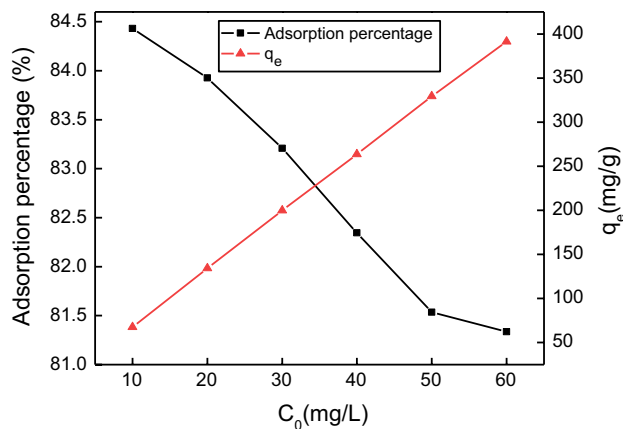


Fig. 11 Effect of the initial concentration of uranyl ions on the adsorption of uranyl ions by FeS@Fe₃O₄ ($m = 10$ mg, $t = 150$ min, pH = 6, $T = 80$ °C, $V = 80$ mL)

adsorbent gradually reaches the adsorption equilibrium, a part of the uranyl ion exists in the free state in the solution, resulting in a decrease in the removal rate but an increase in the adsorption capacity. Since the level of uranium in wastewater is around 35 mg/L, therefore, the concentration of initial uranium (VI) in the subsequent study was selected to be 35 mg/L.

Adsorption kinetic

Pseudo-first-order and pseudo-second-order kinetic models were used to simulate the adsorption of uranyl ions on FeS@Fe₃O₄ and the fitting curves are shown in Fig. 12. The

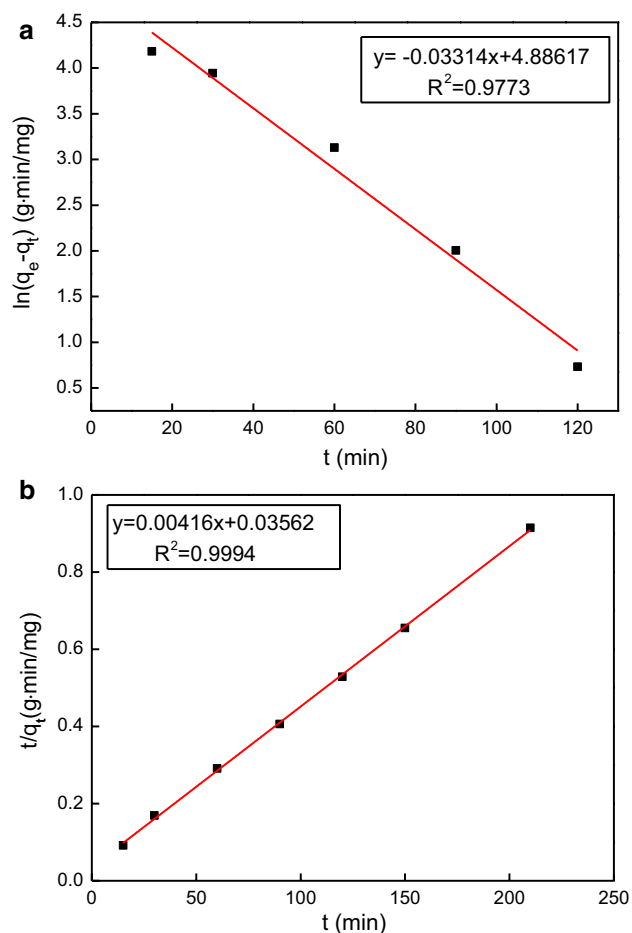


Fig. 12 Linear matches of pseudo-first-order kinetics (a) and pseudo-second-order kinetics (b)

pseudo-first-order kinetic equation and the pseudo-second-order kinetic equation are formulas (3) and (4) respectively [44]:

$$\ln(q_e - q_t) = \ln q_e - K_1 t \quad (3)$$

$$\frac{t}{q_t} = \frac{1}{K_2 q_e^2} + \frac{1}{q_e} t \quad (4)$$

where q_e and q_t are the mass of solute adsorbed by the unit adsorbent in the equilibrium time and t time respectively. K_1 and K_2 are the rate constants of the pseudo-first-order kinetic equation and the pseudo-second-order kinetic equation, respectively.

The fitting parameters are shown in Table 1. It can be seen that the correlation coefficient of the pseudo-second-order kinetic model is 0.9994, the correlation coefficient of the pseudo-first-order kinetic model is 0.9773, and the correlation coefficient of the pseudo-second-order kinetic model is larger than correlation coefficient of the first-order kinetic model. Therefore, this adsorption behavior is more suitable to be described by pseudo-second-order kinetic model, which indicates that the adsorption behavior is dominated by chemical adsorption.

Adsorption isotherm

In order to understand the adsorption behavior of the adsorbent, the adsorption data were analyzed using the Langmuir model (formula 5) and the Freundlich model (formula 6). The two equations are as follows:

$$\frac{C_e}{q_e} = \frac{C_e}{Q_m} + \frac{1}{K_L Q_m} \quad (5)$$

$$\ln q_e = \ln K_F + \frac{1}{n} \ln C_e \quad (6)$$

where q_e (mg/g) and C_e (mg/L) are equilibrium adsorption capacity and equilibrium concentration. Q_m is the maximum adsorption capacity, and K_L is the equilibrium adsorption constant. K_F ($\text{mL}^{1/n} \mu\text{g}^{1-1/n}$) and n are the Freundlich constants. The maximum adsorption capacity (Q_m) can be calculated from the slope of the linear plot of C_e/q_e versus C_e . The values of n and K_F can be obtained from slope of linear plot of $\ln q_e$ versus $\ln C_e$ [45].

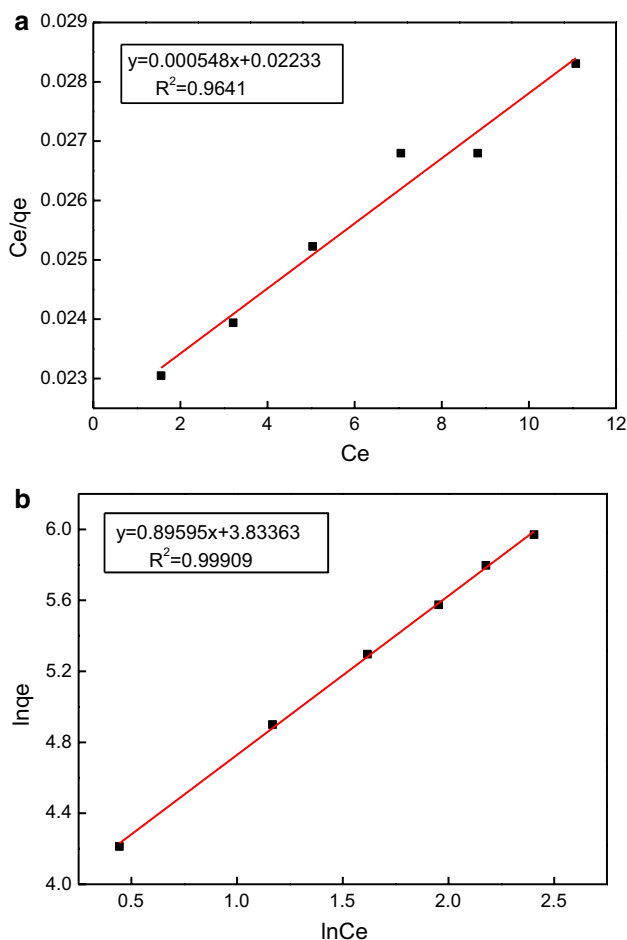
The Langmuir and Freundlich isotherm parameters are shown in Table 2 and the fitting curves are shown in Fig. 13. It is clear that the correlation coefficient of the Freundlich

Table 1 Adsorption kinetic parameter

Temperature (°C)	$q_{e,\text{exp}}$ (mg g ⁻¹)	Pseudo-second-order kinetic model			Pseudo-first-order kinetic model		
		$q_{e,\text{cal}}$ (mg g ⁻¹)	K_2 (g mg ⁻¹ min ⁻¹)	R^2	$q_{e,\text{cal}}$ (mg g ⁻¹)	K_1 (min ⁻¹)	R^2
80	229.03	240.38	0.117	0.9994	132.45	0.033	0.9773

Table 2 Adsorption isotherm model parameter

U (VI) (mg L ⁻¹)	Langmuir isotherm			Freundlich isotherm		
	Q _m (mg g ⁻¹)	K _L (L mg ⁻¹)	R ²	K _F (mL ^{1/n} μg ^{1-1/n})	n	R ²
35	1824.82	0.02	0.9641	46.23	1.116	0.9991

**Fig. 13** Langmuir isotherm of adsorption (a) and Freundlich isotherm of adsorption (b)

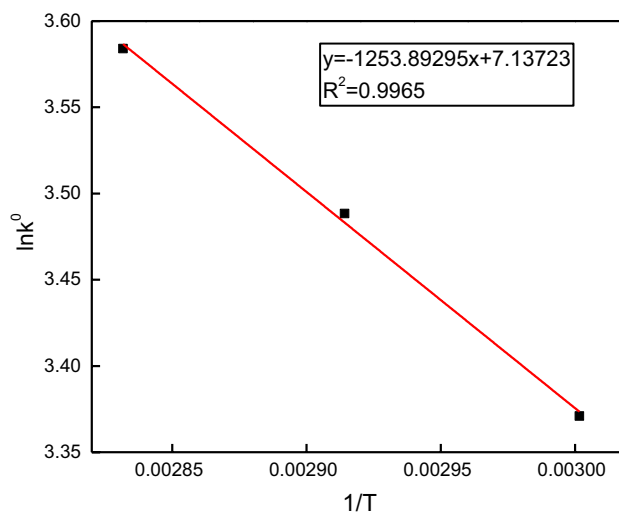
model is 0.9991, which is higher than the correlation coefficient of the Langmuir model ($R^2=0.9641$). The adsorption data agree well with the Freundlich model, indicating that the adsorption of uranyl ions by FeS@Fe₃O₄ is closer to that of multi-molecular layer adsorption [46].

Adsorption thermodynamics

Gibbs free energy (ΔG), enthalpy change (ΔH) and entropy change (ΔS) were calculated by the following three Eqs. (7)–(9), the results are shown in Table 3. Plotting $\ln K^0$ against $1/T$ gives a straight line with slope and intercept equal $-H/R$ and S/R , respectively [47]. The fitting curve of $\ln K^0$ vs $1/T$ is shown in Fig. 14. The results show that:

Table 3 Adsorption thermodynamic parameters

Temperature (°C)	ΔG (kJ mol ⁻¹)	ΔH (kJ mol ⁻¹)	ΔS [J/(mol K)]	R ²
60	-9.34	10.42	59.34	0.9965
70	-9.95			
80	-10.52			

**Fig. 14** Plot of $\ln K^0$ versus $1/T$

$\Delta H > 0$, $\Delta S > 0$, and $\Delta G < 0$. The positive enthalpy (ΔH) indicates that the adsorption process is endothermic and the increase of temperature is beneficial to the adsorption. The entropy change (ΔS) is positive, which reflects the increase of the degree of system confusion. During the adsorption process, the exchanged hydrogen ions diffuse into the solution to form a disordered motion. The decrease in entropy caused by adsorption is less than the increase in entropy caused by disordered motion, resulting in an increase in entropy of the entire system. [48]. The Gibbs free energy (ΔG) is negative, which reflects the adsorption process is a spontaneous.

$$\Delta G = -RT \ln K^0 \quad (7)$$

$$\ln K^0 = \Delta S/R - \Delta H/RT \quad (8)$$

$$K^0 = q_e/C_e \quad (9)$$

where ΔG is the Gibbs free energy (kJ/mol). ΔH is enthalpy change and ΔS is entropy change. R and T are the ideal gas constant [8.314 J/(mol K)] and absolute temperature, respectively. K^0 is adsorption distribution coefficient.

Effect of interfering ions

In order to further study the selective adsorption of uranyl ions on the adsorbent, the effects of the interfering ions were investigated. Industrial wastewater contains a variety of metal ions, including Na^+ , K^+ , Ni^{2+} , Mg^{2+} , Zn^{2+} , Al^{3+} , Fe^{2+} , Ca^{2+} , Cu^{2+} and so on. So we chose randomly the five metal ions (Ni^{2+} , Mg^{2+} , Zn^{2+} , Al^{3+} and Cu^{2+}) in these above metal ions as interfering ions and applied in the experiment. As shown in Fig. 15, Ni^{2+} , Mg^{2+} , Zn^{2+} and Cu^{2+} had certain effect on the adsorption when the concentration of these cations reached to 20 mg/L, however, when the concentration of Ni^{2+} , Mg^{2+} and Zn^{2+} increased, the adsorption capacity remained about 227 mg/g. When the concentration of Cu^{2+} increased to 45 mg/L, the adsorption capacity of $\text{FeS@Fe}_3\text{O}_4$ on uranyl ions decreased from 227 to 226.6 mg/L. When the concentration of Al^{3+} was lower than 20 mg/L, it had no influence on the adsorption. When the concentration of Al^{3+} increased, the adsorption capacity of $\text{FeS@Fe}_3\text{O}_4$ on uranyl ions only decreased from 229.0 to 226.6 mg/g.

Reusability of $\text{FeS@Fe}_3\text{O}_4$

To test the reusability of $\text{FeS@Fe}_3\text{O}_4$, five successive adsorption and desorption cycles were performed. The results are shown in Fig. 16. It is obvious that the adsorption rate of $\text{FeS@Fe}_3\text{O}_4$ only decreased from 83.2 to 80.6% after 5 adsorption–desorption operations, so the reusability of $\text{FeS@Fe}_3\text{O}_4$ can be convincingly proved.

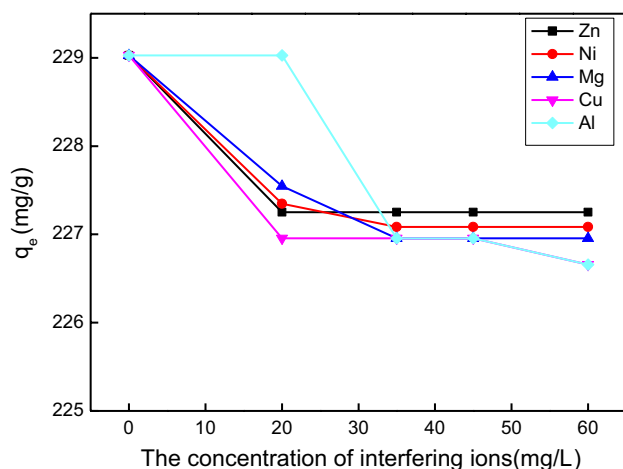


Fig. 15 Effect of coexisting interfering ions on the adsorption of uranyl ions by $\text{FeS@Fe}_3\text{O}_4$ (pH=6, m = 10 mg, T = 80 °C, C_0 = 35 mg/L, t = 150 min, V = 80 mL)

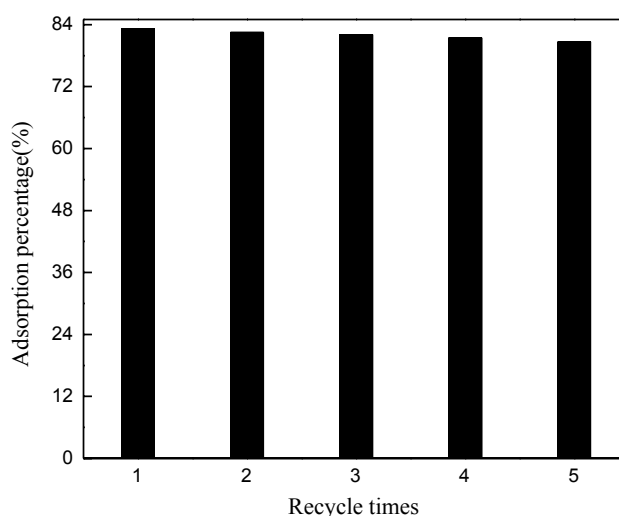


Fig. 16 Reusability of the $\text{FeS@Fe}_3\text{O}_4$ for uranyl ions adsorption

Conclusion

In this paper, core–shell magnetic nanoparticles of $\text{FeS@Fe}_3\text{O}_4$ were successfully prepared by the ultrasonic-assisted method. The average diameter of the nanoparticles is about 30 nm, and the saturation magnetic field intensity is 57.18 emu/g, and it has better superparamagnetism. The prepared adsorbents have good adsorption performance for uranyl ions. The optimum adsorption conditions were as follows: pH = 6, temperature 80 °C, initial uranium concentration 35 mg/L, contact time 2.5 h, adsorbent dosage 10 mg. Under optimal conditions, the adsorption capacity can reach 229.03 mg/g. The experimental results show that the adsorption kinetics accords with the pseudo second order kinetic model, the fitting degree of R^2 is 0.9994. The adsorption isotherm is in accordance with the Freundlich isothermal adsorption model, and the fitting degree of R^2 is 0.9991. The research of adsorption thermodynamics shows that the adsorption process is endothermic and spontaneous. Interference experiments and adsorption desorption cycle experiments proved that the prepared $\text{FeS@Fe}_3\text{O}_4$ had good selective adsorption and reuse performance for uranyl ions.

Acknowledgements This study was financially supported by Hunan Engineering Laboratory for Preparation Technology of Polyvinyl Alcohol Fiber Material, Huaihua University (HGY201805) and the Natural Science Foundation of Hunan Province (2017JJ2231).

Compliance with ethical standards

Conflict of interest All the authors do not have any possible conflicts of interest.

References

- Feng ML, Sarma D, Qi X, Du KZ, Huang XY, Kanatzidis MG (2016) Efficient removal and recovery of uranium by a layered organic-inorganic hybrid thiostannate. *J Am Chem Soc* 138(38):12578–12585
- Tavengwa NT, Cukrowska E, Chimuka L (2015) Sequestration of U(VI) from aqueous solutions using precipitate ion imprinted polymers endowed with oleic acid functionalized magnetite. *J Radioanal Nucl Chem* 304(2):933–943
- Gong Y, Tang J, Zhao D (2016) Application of iron sulfide particles for groundwater and soil remediation: a review. *Water Res* 89:309–320
- Liu R, Yang Z, He Z, Wu L, Hu C, Wu W, Qu J (2016) Treatment of strongly acidic wastewater with high arsenic concentrations by ferrous sulfide (FeS): inhibitive effects of S(0)-enriched surfaces. *Chem Eng J* 304:986–992
- Suzuki T, Kawasaki T, Takao K, Harada M, Nogami M, Ikeda Y (2012) A study on selective precipitation ability of cyclic urea to U(VI) for developing reprocessing system based on precipitation method. *J Nucl Sci Technol* 49(10):1010–1017
- Tran TK, Leu HJ, Chiu KF, Lin CY (2017) Electrochemical treatment of heavy metal-containing wastewater with the removal of COD and heavy metal ions. *J Chin Chem Soc* 64(5):493–502
- Chen L, Bai Z, Zhu L, Zhang L, Cai Y, Li Y, Liu W, Wang Y, Chen L, Diwu J (2017) Ultrafast and efficient extraction of uranium from seawater using an amidoxime appended metal-organic framework. *ACS Appl Mater Interfaces* 9(38):32446–32451
- Endrizzi F, Leggett C, Rao L (2016) Scientific basis for efficient extraction of uranium from seawater, I: understanding the chemical speciation of uranium under seawater conditions. *Ind Eng Chem Res* 55(15):4249–4256
- Wang LL, Luo F, Dang LL, Li JQ, Wu XL, Liu SJ, Luo MB (2015) Correction: ultrafast high-performance extraction of uranium from seawater without pretreatment using an acylamide- and carboxyl-functionalized metal-organic framework. *J Mater Chem A* 3(34):17880
- Zhe X, Jiangtao HU, Wang MH, Zhang WL, Shineng LI, Gao QH, Guozhong WU (2013) Properties and evaluation of amidoxime-based UHMWPE fibrous adsorbent for extraction of uranium from seawater. *Sci China Chem* 56(11):1504–1509
- Hoyer M, Zabelt D, Steudtner R, Brendler V, Haseneder R, Repke JU (2014) Influence of speciation during membrane treatment of uranium contaminated water. *Sep Purif Technol* 132:413–421
- Torkabad MG, Keshtkar AR, Safdari SJ (2017) Comparison of polyethersulfone and polyamide nanofiltration membranes for uranium removal from aqueous solution. *Prog Nucl Energy* 94:93–100
- Ma H, Hsiao BS, Chu B (2013) Ultrafine cellulose nanofibers as efficient adsorbents for removal of UO_2^{2+} in water. *ACS Macro Lett* 1(1):213–216
- Sprynskyy M, Kowalkowski T, Tutu H, Cukrowska EM, Buszewski B (2011) Adsorption performance of talc for uranium removal from aqueous solution. *Chem Eng J* 171(3):1185–1193
- Kaynar ÜH, Ayvacıklı M, Kaynar ŞÇ, Hiçsönmez Ü (2014) Removal of uranium(VI) from aqueous solutions using nanoporous ZnO prepared with microwave-assisted combustion synthesis. *J Radioanal Nucl Chem* 299(3):1469–1477
- Jing L, Lei Z, Dong F, Hudson-Edwards KA (2016) Enhancing As(V) adsorption and passivation using biologically formed nano-sized FeS coatings on limestone: implications for acid mine drainage treatment and neutralization. *Chemosphere* 168:529–538
- Liu X, Ai L, Jiang J (2015) Interconnected porous hollow CuS microspheres derived from metal-organic frameworks for efficient adsorption and electrochemical biosensing. *Powder Technol* 283:539–548
- Qu Z, Yan L, Li L, Xu J, Liu M, Li Z, Yan N (2014) Ultraeffective ZnS nanocrystals sorbent for mercury(II) removal based on size-dependent cation exchange. *ACS Appl Mater Interfaces* 6(20):18026–18032
- Wolthers M, Charlet L, Linde PRvD, Rickard D, Weijden CHvD (2005) Surface chemistry of disordered mackinawite (FeS). *Geochim Cosmochim Acta* 69(14):3469–3481
- Watson JHP, Ellwood DC, Deng Q, Mikhailovsky S, Hayter CE, Evans J (1995) Heavy metal adsorption on bacterially produced FeS. *Miner Eng* 8(10):1097–1108
- Fang L, Li L, Qu Z, Xu H, Xu J, Yan N (2018) A novel method for the sequential removal and separation of multiple heavy metals from wastewater. *J Hazard Mater* 342:617–624
- Sun Y, Liu Y, Lou Z, Yang K, Lv D, Zhou J, Xu X (2018) Enhanced performance for Hg(II) removal using biomaterial (CMC/gelatin/starch) stabilized FeS nanoparticles: stabilization effects and removal mechanism. *Chem Eng J* 344:616–624
- Dzade NY, Roldan A, Leeuw NHD (2017) Structures and properties of As(OH)₃ adsorption complexes on hydrated mackinawite (FeS) surfaces: a DFT-D2 study. *Environ Sci Technol* 51(6):3461–3470
- Shao D, Ren X, Wen J, Hu S, Xiong J, Jiang T, Wang X, Wang X (2016) Immobilization of uranium by biomaterial stabilized FeS nanoparticles: effects of stabilizer and enrichment mechanism. *J Hazard Mater* 302:1–9
- Sun Y, Lou Z, Yu J, Zhou X, Lv D, Zhou J, Baig SA, Xu X (2017) Immobilization of mercury (II) from aqueous solution using Al₂O₃-supported nanoscale FeS. *Chem Eng J* 323:483–491
- Chen L, Zhao D, Chen S, Wang X, Chen C (2016) One-step fabrication of amino functionalized magnetic graphene oxide composite for uranium(VI) removal. *J Colloid Interface Sci* 472:99–107
- Yan LG, Yang K, Shan RR, Yan T, Wei J, Yu SJ, Yu HQ, Du B (2015) Kinetic, isotherm and thermodynamic investigations of phosphate adsorption onto core-shell Fe₃O₄@LDHs composites with easy magnetic separation assistance. *J Colloid Interface Sci* 448:508–516
- Zhang D, Gao G, Ma W, Zhu J, Qiu G, Liu X (2013) Facile synthesis and properties of bifunctional magnetic-optical Fe₃O₄@ZnS nanocomposites with core-shell structure. *Appl Mech Mater* 320:92–98
- Zhao D, Zhang Q, Xuan H, Chen Y, Zhang K, Feng S, Alsaedi A, Hayat T, Chen C (2017) EDTA functionalized Fe₃O₄/graphene oxide for efficient removal of U(VI) from aqueous solutions. *J Colloid Interface Sci* 506:300–307
- Tavengwa NT, Cukrowska E, Chimuka L (2016) Modeling of adsorption isotherms and kinetics of uranium sorption by magnetic ion imprinted polymers. *Toxicol Environ Chem Res* 98(1):1–12
- Kera NH, Bhaumik M, Pillay K, Ray SS, Maity A (2017) Selective removal of toxic Cr(VI) from aqueous solution by adsorption combined with reduction at a magnetic nanocomposite surface. *J Colloid Interface Sci* 503:214–228
- Yu Y, Yu L, Shih K, Chen JP (2018) Yttrium-doped iron oxide magnetic adsorbent for enhancement in arsenic removal and ease in separation after applications. *J Colloid Interface Sci* 521:252–260
- Zhang S, Zhang Y, Liu J, Xu Q, Xiao H, Wang X, Xu H, Zhou J (2013) Thiol modified Fe₃O₄@SiO₂ as a robust, high effective, and recycling magnetic sorbent for mercury removal. *Chem Eng J* 226(24):30–38
- Iranmanesh P, Saeednia S, Mehran M, Dafeh SR (2016) Modified structural and magnetic properties of nanocrystalline MnFe₂O₄ by pH in capping agent free co-precipitation method. *J Magn Magn Mater* 425:31–36

35. Xu Y, Ke G, Yin J, Lei W, Yang P (2019) Synthesis of thiol-functionalized hydrotalcite and its application for adsorption of uranium (VI). *J Radioanal Nucl Chem* 319(3):791–803
36. Wang CF, Liu ZR, Xue GR, Lei Y, Wang Y, Zhou LM (2016) Adsorptive properties of sunflower seed shells for UO_2^{2+} in aqueous solution. *J Nucl Radiochem* 38(2):107–115
37. Gholizadeh A, Jafari E (2017) Effects of sintering atmosphere and temperature on structural and magnetic properties of Ni-Cu-Zn ferrite nano-particles: magnetic enhancement by a reducing atmosphere. *J Magn Magn Mater* 422:328–336
38. Ma YX, Xing D, Shao WJ, Du XY, La PQ (2017) Preparation of polyamidoamine dendrimers functionalized magnetic graphene oxide for the adsorption of Hg(II) in aqueous solution. *J Colloid Interface Sci* 505:352–363
39. Li SL, Zhou YP, Liu JJ (2016) *Physical chemistry (2009)*, 5th edn. Higher Education Press, Beijing, pp 594–595
40. Gao Y, Yuan Y, Ma D, Li L, Li Y, Xu W, Tao W (2014) Removal of aqueous uranyl ions by magnetic functionalized carboxymethylcellulose and adsorption property investigation. *J Nucl Mater* 453(1–3):82–90
41. Dolatyari L, Yaftian MR, Rostamnia S (2016) Removal of uranium(VI) ions from aqueous solutions using Schiff base functionalized SBA-15 mesoporous silica materials. *J Environ Manage* 169:8–17
42. Lu BQ, Li M, Zhang XW, Huang CM, Wu XY, Fang Q (2018) Immobilization of uranium into magnetite from aqueous solution by electrodepositing approach. *J Hazard Mater* 343:255–265
43. Sepehrian H, Asadi Z (2012) Studies on the recovery of uranium from nuclear industrial effluent using nanoporous silica adsorbent. *Int J Environ Sci Technol* 9(4):629–636
44. Zhou L, Shang C, Liu Z, Huang G, Adesina AA (2012) Selective adsorption of uranium(VI) from aqueous solutions using the ion-imprinted magnetic chitosan resins. *J Colloid Interface Sci* 366(1):165–172
45. Qian J, Zhang S, Zhou Y, Dong P, Hua D (2014) Synthesis of surface ion-imprinted magnetic microspheres by locating polymerization for rapid and selective separation of uranium(VI). *RSC Adv* 5(6):4153–4161
46. Khani R, Sobhani S, Beyki MH (2016) Highly selective and efficient removal of lead with magnetic nano-adsorbent: multivariate optimization, isotherm and thermodynamic studies. *J Colloid Interface Sci* 466:198–205
47. Donia AM, Atia AA, El-Boraey H, Mabrouk DH (2006) Uptake studies of copper(II) on glycidyl methacrylate chelating resin containing Fe_2O_3 particles. *Sep Purif Technol* 49(1):64–70
48. Zhang X, Wang J, Li R, Dai Q, Gao R, Liu Q, Zhang M (2013) Preparation of $\text{Fe}_3\text{O}_4@\text{C}$ @layered double hydroxide composite for magnetic separation of uranium. *Ind Eng Chem Res* 52(30):10152–10159

Publisher's Note Springer Nature remains neutral with regard to jurisdictional claims in published maps and institutional affiliations.